



Long-range influence of manipulating disordered insulators locallyZ. Ovadyahu *Racah Institute of Physics, The Hebrew University, Jerusalem 91904, Israel* (Received 25 November 2019; revised manuscript received 19 January 2020; accepted 20 February 2020; published 13 March 2020)

Localization of wave functions is arguably the most familiar effect of disorder in quantum systems. It has been recently argued [V. Khemani, R. Nandkishore, and S. L. Sondhi, *Nat. Phys.* **11**, 560 (2015)] that, contrary to naive expectation, manipulation of a localized site in the disordered medium may produce a disturbance over a length scale much larger than the localization length, ξ . Here we report on the observation of this nonlocal phenomenon in electronic transport experiments. Being a wave property, visibility of this effect hinges upon quantum coherence, and its spatial scale may be ultimately limited by the phase-coherent length of the disordered insulator. Evidence for quantum coherence in the Anderson-insulating phase may be obtained from magnetoresistance measurements which, however, are useful mainly in thin films. The technique used in this work offers an empirical method to measure this fundamental aspect of Anderson insulators even in relatively thick samples.

DOI: [10.1103/PhysRevB.101.094202](https://doi.org/10.1103/PhysRevB.101.094202)**I. INTRODUCTION**

Disorder may lead to a variety of nontrivial phenomena in both classical and quantum systems. The most familiar of these phenomena is Anderson localization [1]. This phenomenon has been established in electronic transport [2], in propagation of light [3] and sound waves [4], and in disordered Bose-Einstein condensates [5].

Localization of wave functions may seem a way to allow manipulation of a particular site in a solid while parts of the system that are remote from it are unaffected. This expectation has been recently questioned; Khemani, Nandkishore, and Sondhi (KNS) [6] have shown that adiabatically changing the potential on a local site will produce an effect over a distance that may exceed the localization length ξ by a considerable margin. This long-range effect may have important consequences for quantum-computing manipulations and for fundamental issues such as the orthogonality catastrophe [6,7].

In this work we describe a method that allows observation of the KNS effect in an electronic system and show results that demonstrate the quantum nature of the phenomenon.

II. EXPERIMENTAL**A. Sample preparation**

The samples used in this study were amorphous indium oxide (In_xO) made by e-gun evaporation of 99.999% pure $\text{In}_2\text{O}_{3-x}$ onto room-temperature Si wafers under a partial pressure of 1.3×10^{-4} mbar of O_2 and at a rate of 0.3 ± 0.1 Å/s. Under these conditions the carrier concentration N of the samples, measured by the Hall effect at room temperatures, was $N \approx (1 \pm 0.1) \times 10^{19} \text{ cm}^{-3}$. Using a free-electron formula, this carrier-concentration is associated with $\partial n / \partial \mu \approx 10^{32} \text{ erg}^{-1} \text{ cm}^{-3}$. The Si wafers (boron-doped with bulk resistivity $\rho \leq 2 \times 10^{-3} \text{ } \Omega \text{ cm}$) were employed as the

gate electrode in the field-effect experiments. A thermally grown SiO_2 layer, $2 \text{ } \mu\text{m}$ thick, served as the spacer between the sample and the conducting Si:B substrate. Film thickness was measured *in situ* by a quartz-crystal monitor calibrated against x-ray reflectometry. Sample geometry was defined by the use of a stainless-steel mask during deposition into rectangular strips that were $0.8 \pm 0.1 \text{ mm}$ wide and $1 \pm 0.1 \text{ mm}$ long.

B. Measurement techniques

Conductivity of the samples was measured using a two-terminal ac technique employing a 1211 ITHACO current preamplifier and a PAR 124A lock-in amplifier using frequencies of 30–75 Hz depending on the RC of the sample-gate structure. R is the source-drain resistance and C is the capacitance between the sample and the gate (C in our samples was typically $\cong 10^{-10} \text{ F}$ and R for the samples studied in this work ranged between 1.5 and 20 M Ω). Except when otherwise noted, the ac voltage bias in conductivity measurements was small enough to ensure near-ohmic conditions. Most measurements were performed with the samples immersed in liquid helium at $T \approx 4.1 \text{ K}$ held by a 100-liter storage dewar. This allowed up to 2 months of measurements on a given sample while keeping it cold (and in the dark). These conditions are essential for measurements where extended times of relaxation processes are required at a constant temperature. All samples described below were Anderson insulating and exhibited hopping conductivity σ that for $4 < T < 50 \text{ K}$ was of the Mott form [8],

$$\sigma(T) \approx \exp[-(T_0/T)^{1/4}], \quad (1)$$

as illustrated in Fig. 1 for two typical samples. This allowed an estimate of the localization length ξ through [8]: $k_B T_0 \approx (\xi^3 \partial n / \partial \mu)^{-1}$, where $\partial n / \partial \mu$ is the thermodynamic density of states. With $\partial n / \partial \mu \approx 10^{32} \text{ erg}^{-1} \text{ cm}^{-3}$, the ξ values for the

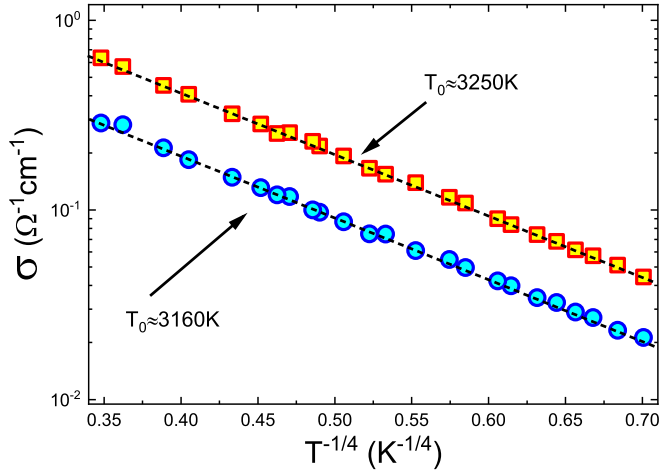


FIG. 1. Conductivity versus temperature for two In_xO samples from the same preparation batch with thickness $d = 82$ nm. These exhibit Mott variable-range hopping, yielding similar activation energies T_0 and localization lengths of $\xi \approx 3$ nm (see text for details).

samples reported below ranged between 2.7 and 3.3 nm. These ξ values are close to the intercarrier distance $N^{-1/3}$ of this version of In_xO as may be expected for samples that are far from the metal-insulating transition which applies to all our studied samples. This makes the estimate for ξ , based on the $\sigma(T)$ data, a plausible value.

Taking the sample far from equilibrium to study its thermalization dynamics is accomplished in this work by exposing the sample to an AlGaAs diode operating at $\approx 0.82 \pm 0.05$ μm mounted on the sample-stage ≈ 10 – 15 mm from the sample. The diode was energized by a computer-controlled Keithley 220 current source. Upon exposure to the infrared source, the electrons are promptly raised to a high-energy state and their excess energy is then dissipated into the phonon system (a radiationless process [9]). In this method, only the sample is efficiently heated and its excess energy is uniformly distributed throughout the sample much faster than the timescale of the experiments described below. Full details of this technique and its application for the study of several Anderson insulators are described in Ref. [9].

III. RESULTS AND DISCUSSION

In a field-effect experiment, the charge δQ added to the sample when the gate voltage is changed by δV_g , resides in a thin layer of thickness $\lambda \approx (4\pi e^2 \partial n / \partial \mu)^{-1/2}$ at the interface between the sample and the spacer [10,11] (The dielectric constant of the material κ is of the order of 10). The thickness of this layer in In_xO is $\lambda \approx 2$ nm, which is much smaller than the thickness d of the samples studied in this work that ranged between 45 and 150 nm. Yet, it turns out that the added charge δQ to the system due to δV_g had an effect extending over length scales much longer than both λ and ξ .

This observation may be inferred from $G(V_g)$ plots, taken at different times t_Q , while the sample is relaxing after being quenched cooled from an excited state; consider the $G(t, V_g)$ plots for the samples in Fig. 2. The protocol used throughout the series of measurements shown in this composite figure was

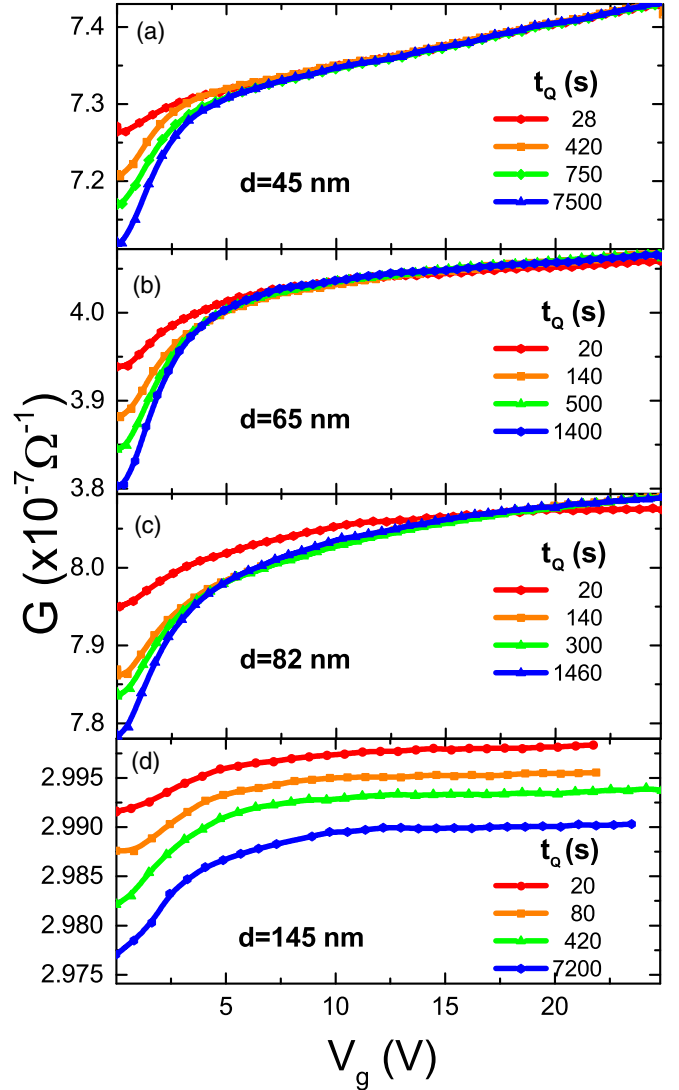


FIG. 2. Results of the $G(t, V_g)$ protocol performed on In_xO samples with similar compositions (carrier concentration of $\approx 10^{19} \text{ cm}^{-3}$) but different thicknesses d . Each $G(V_g)$ plot was obtained with the same sweep rate $\partial V_g / \partial t = 0.5$ V/s. Bath temperature $T = 4.1$ K.

as follows. The sample, immersed in liquid He at $T = 4.11$ K, was exposed for 3 s to an infrared source (light-emitting diode at 0.82 - μm radiation) taking it from equilibrium. $G(V_g)$ scans were then taken with constant $\partial V_g / \partial t$ starting from $V_g = 0$, at which the gate voltage was kept between subsequent scans. These are labeled in the graphs by the time t_Q that elapsed since turning off the infrared source (and the onset of relaxation towards restoring equilibrium under $V_g = 0$). Each of these $G(V_g)$ plots reflects the energy dependence of $\partial n / \partial \mu$ modulated by a “memory dip” which results from the interplay between disorder and Coulomb interaction [12].

Note first the difference between the thinnest and thickest samples in the series [Figs. 2(a) and 2(d), respectively]. In the former, the $G(V_g)$ plots taken at different times tend to merge for $V_g \geq 10$ V, while, for the 145-nm sample, they tend to become parallel.

A simple explanation to the results exhibited by the sample in Fig. 2(d) is that the added charge only affects the part of the

sample that is close to the spacer interface while the rest of it is unaffected. In this case the sample is effectively composed of two conductors in parallel: one where the $G(t, V_g)$ curves are like the pattern exhibited by the sample in Fig. 2(a), and another for which $G(t)$ just monotonically decreases after the quantum quench, independent of δV_g . Superimposing these two components qualitatively reproduces the $G(t, V_g)$ curves exhibited by the 145-nm sample in Fig. 2(d).

It is important to understand the different roles played by the infrared exposure versus the gate sweeps in these experiments. Changing the gate voltage or exposing the sample to an infrared source will take the system from equilibrium. However, these agents do not play a symmetric role in the protocol; the infrared exposure is a one-shot event driving the system far from equilibrium. Sweeping the gate is used to take a snapshot of how far the system is on its relaxation trail. This is done intermittently as time progresses and yields a certain swing $\delta G(t)$ reflecting the development of a memory dip. This δG may then be compared with the background conductance value that is going down with time due to the original excitation by the infrared source (which, as alluded to in Sec. III, affects the entire thickness of the sample). The form of the observed $G(t, V_g)$ plots will tell whether or not the gate sweeping affects the entire sample volume [as in Figs. 2(a)–2(c)] or only part of it [as in Fig. 2(d)].

The $G(t, V_g)$ curves pattern characteristic of a thin sample was observed in Ref. [13] on crystalline indium oxide and later in Ref. [14] on a version of In_xO different than the one used here (namely, with $N \approx 8 \times 10^{19} \text{ cm}^{-3}$).

To account for the behavior of the three thinner samples is a more challenging task; apparently in these instances the disturbance caused by the added charge extends throughout their entire thickness—over a length scale of d which, for the 82-nm sample, is 25 to 30 times larger than the localization length ξ . It is hard to see how such a long-range effect is possible unless the wave function overlap that is $L \gg \xi$ apart is much better than might be expected from exponential decay. The Coulomb interaction due to δQ over this length scale, even if unscreened, is too weak relative to the local disorder to affect $G(V_g)$ during the time V_g is swept.

High-transmission channels through disordered media would offer an explanation for the long-range effect. These resonant channels are theoretically possible but exponentially rare [15–17]. By contrast, the scenario proposed by KNS creates such resonant channels in the disordered system with high probability by using a time-dependent adiabatic process [6]. Adapted for our geometry, quasiextended states are parametrically formed perpendicular to the film plane by slowly varying the local potential V at the interface layer. As we now shown, this scenario accounts for all aspects of the experimental results.

Let us first look at r_{zd} , the extent of the “zone of disturbance” expected of the KNS-produced resonances [6]:

$$r_{zd} \approx \xi \ln \left(\frac{W^2}{\partial V / \partial t \hbar} \right). \quad (2)$$

With the value of the quenched disorder in our samples [18] $W \approx 0.5\text{--}1 \text{ eV}$, the rate of potential-change [19] $\partial V / \partial t \approx 0.5 \text{ meV/s}$, and $\xi \approx 3 \text{ nm}$, Eq. (1) gives $r_{zd} \approx 100 \text{ nm}$.

Note that $r_{zd} \approx 100 \text{ nm}$ is consistent with our results (Fig. 1); it is close to the film thickness below which the $G(t, V_g)$ curves converge at high gate voltages, which implies $r_{zd} \geq d$. In addition, the mean values that δV attains in the V_g interval used in the experiments covers the energy separation $\delta E \approx (\partial n / \partial \mu L^3)^{-1}$ for states that are apart by any $L \gtrsim 2\xi$. This secures an ample “tuning margin” for creating the quasiextended states by the KNS scenario.

A fundamental requirement of the KNS mechanism is that phase coherence must be preserved throughout the spatial-scale in question. This requirement follows from the quantum-mechanical nature of the process. In other words, the range of disturbance may be r_{zd} in Eq. (1) *only* when L_ϕ , the phase-coherent length in the medium obeys $L_\phi > r_{zd}$.

Evidence for phase coherence in Anderson-localized films over scales of tens of several nanometers has been reported. This evidence is based on two phenomena, both strictly requiring phase coherence: orbital magnetoconductance [20,21] and Andreev tunneling [22]. The latter, performed on In_xO films of a composition similar to that used in the current work, demonstrated that a coherence length of $\simeq 60 \text{ nm}$ at $T \approx 4 \text{ K}$ is realizable in this system.

A further test of the role of quantum coherence in the nonlocal effect discussed here is to see how the $G(t, V_g)$ plots change when dephasing is judiciously introduced. Once the dephasing rate is large enough to cause $L_\phi < d$, the resulting $G(t, V_g)$ plots should revert from the “converging” pattern to that resembling the results in Fig. 1(d).

To implement this test in a controlled way, one needs a dephasing agent that can be turned on and off at will. An effective and easy way to control the mechanism for dephasing Anderson insulators is using a non-ohmic field in the transport measurement [20]. This has been demonstrated in magnetoconductance measurements on strongly localized indium oxide films [20]. This technique was applied on three different In_xO samples and the results corroborate the expected behavior caused by the extra dephasing. Figure 3 illustrates the results of one of these experiments:

Figure 3(a) shows a set of $G(t, V_g)$ curves taken in linear response. These “converging” plots are consistent with $r_{zd} > d$. Using non-ohmic V_{SD} for measuring $G(V_g)$ on the same sample produced, however, different results; the $G(t, V_g)$ curves [Fig. 3(b) and 3(c)] resemble the pattern obtained for the thick sample in Fig. 2(d) where presumably the range of δV_g is smaller than the sample thickness.

Another indication that, under the higher V_{SD} conditions, part of the sample is not affected by the gate voltage is shown in Fig. 4. This figure compares the relative magnitude of the memory dips taken under the same fields used in Figs. 3(a)–3(c). The figure shows a large reduction in the memory-dips’ magnitude for the two non-ohmic V_{SD} used relative to the linear-response plot. The reduced range of disturbance implied by the data in Figs. 3(b), 3(c) and 4 is consistent with the dephasing effect of non-ohmic fields causing L_ϕ to become the shortest scale. Similar behavior was observed on two other samples with $d = 65 \text{ nm}$ and $d = 82 \text{ nm}$ upon application of non-ohmic fields.

For further discussion of the results of the non-ohmic fields, we show in Fig. 5 resistance versus source-drain voltage V_{SD} plots for three of the samples used in this study.

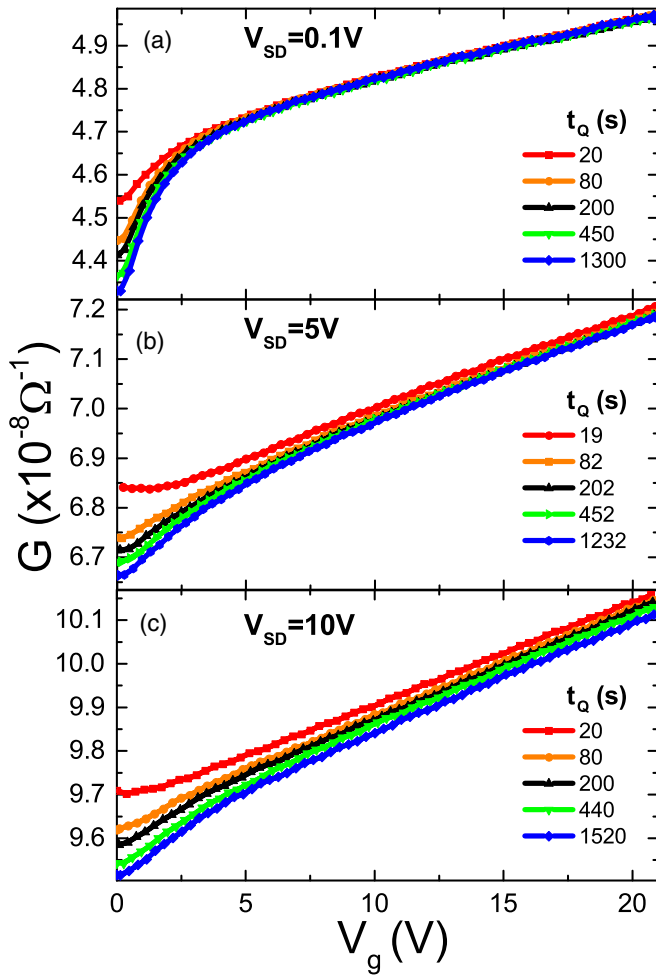


FIG. 3. Results of the $G(t, V_g)$ protocol applied on a single 65-nm-thick In_xO sample under different source-drain fields (distance between the source-drain contacts is 1 mm). Panel (a) shows the results of the protocol taken under linear-response conditions while in panels (b) and (c) the $G(t, V_g)$ plots were taken using non-ohmic voltages in the measurement causing the somewhat enhanced conductance. The bath temperature was $T = 4.1$ K.

Note first that the increase in the overall conductance of the sample used in Fig. 3 under V_{SD} of 5 and 10 V (by a factor of ≈ 1.5 and ≈ 2 , respectively, see Fig. 5) is not the reason for the qualitative change in the $G(t, V_g)$ plots; when measured in linear response, samples with the same d , but conductance that differed by as much as an order of magnitude, still exhibited the same converging $G(t, V_g)$ curves. Second, in terms of dephasing, the effect of a non-ohmic field acts in the same direction as a higher sample temperature [20]. The increase of the effective temperature ΔT due to the applied source-drain field F_{SD} may be roughly estimated as $\Delta T \approx e\xi F_{SD}/k_B$, which for the $F \approx 10 \text{ V m}^{-1}$ used in Fig. 3(c) is tantamount to $\Delta T \approx 0.1\text{--}0.3$ K.

That L_ϕ in an Anderson insulator may be ≥ 82 nm at $T \approx 4$ K, implicit to our proposed picture, is not an obvious fact, it deserves some elaboration; to put things in perspective, L_ϕ of this order of magnitude is typical of *diffusive* samples at this temperature [23]. This may conflict with common intuition expecting disorder to decrease transport-related spatial scales.

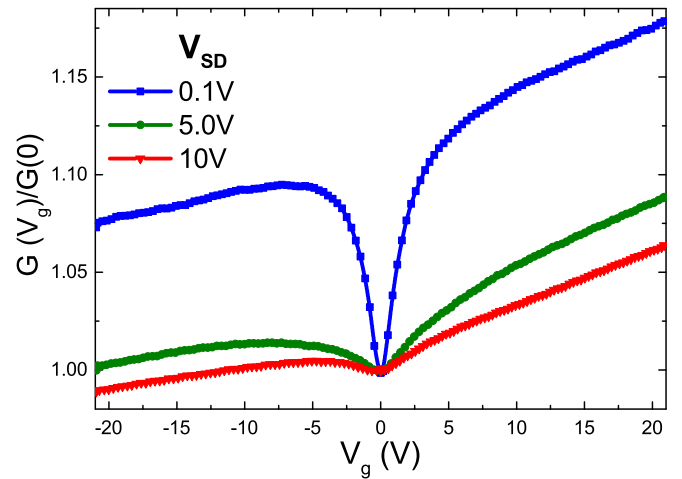


FIG. 4. The memory dips taken under the same source-drain voltages and sweep rates as the data in Fig. 2. These were taken, in each case, after the sample was allowed to relax at $V_g = 0$ V for 24 h. The bath temperature was $T = 4.1$ K.

However the dependence of L_ϕ on disorder is not clear even in diffusive systems despite extensive studies [24], let alone in the more intricate Anderson-insulating phase where this issue has barely been studied. On the basis of current knowledge it is not impossible that L_ϕ in the insulating phase be as large as that in the metallic phase. In terms of mechanisms, the insulating phase may even have an advantage; electron-electron inelastic scattering that, at low temperatures, is the main source of dephasing in diffusive systems is suppressed in the insulating phase. This has been anticipated on theoretical grounds [24] and has been shown experimentally [25]. Moreover, the electron-phonon inelastic rate is likely also suppressed due to the reduced overlap between the initial and final electronic states involved in the inelastic event. Therefore dephasing due to inelastic scattering may actually

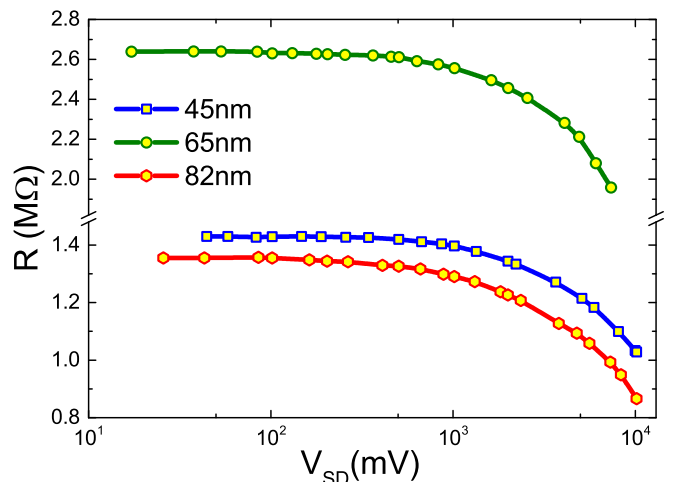


FIG. 5. Sample resistance as a function of the source-drain voltage V_{SD} . Plots are given for three samples labeled by their thickness. The nominal field used for ohmic-regime measurement was typically $F = 1 \text{ V m}^{-1}$. The source-drain separation for all these samples was 1 mm. The upper plot is taken on the same sample as in Fig. 3 above.

be weakened in the strongly localized regime. On the other hand, once interactions are turned on, a potential source for dephasing appears that may not have existed in the weak-disorder regime: spin-flips. This mechanism may become important once the on-site Coulomb repulsion is strong enough to precipitate a finite density of singly occupied states at the Fermi energy [26]. These singly occupied sites act like local magnetic impurities and may contribute to dephasing [27]. This potential source of dephasing may be the reason for the paucity of experiments reporting on quantum-interference effects in Anderson insulators in systems that do exhibit such effects in their diffusive regime. Evidence for quantum-coherent effects is usually based on observation of anisotropic magnetoconductance. This technique, however, becomes ineffective for films thicker than a few tens of nanometers [21], a weakness not shared by our protocol.

In sum, we demonstrated the existence of a nonlocal effect in strongly disordered Anderson insulators extending over surprisingly long spatial scales. It was shown that this effect is consistent with the mechanism proposed by KNS. The study also revealed that this spatial scale is limited by the phase-coherent length of the medium. Therefore the KNS effect is

expected to be considerably weakened by temperature while being only logarithmically sensitive to the rate dependence of a local potential change. Inasmuch as dephasing is dominated by inelastic scatterings, the phase-coherent length in the insulating phase may be longer than intuitively expected. This is actually a natural outcome of localization-induced discreteness. In the presence of on-site interaction however, spin effects may become important and phase coherence could be compromised, even in the absence of inelastic events, depending on the nature of the spin system [27]. The nonequilibrium technique employed in this study may offer a way to experimentally study these fundamental issues of disordered quantum systems.

ACKNOWLEDGMENTS

The author is grateful for the stimulating discussions with participants in the “The Dynamics of Quantum Information” program held in 2018 at the Kavli Institute, Santa Barbara. This research has been supported by Grant No. 1030/16 administered by the Israel Academy for Sciences and Humanities.

-
- [1] P. W. Anderson, Absence of diffusion in certain random lattices, *Phys. Rev.* **109**, 1492 (1958).
- [2] B. Kramer and A. MacKinnon, Localization: Theory and experiment, *Rep. Prog. Phys.* **56**, 1469 (1993), and references therein.
- [3] S. Diederik Wiersma, P. Bartolini, A. D. Lagendijk, and R. Righini, Localization of light in a disordered medium, *Nature (London)* **390**, 671 (1997).
- [4] H. Hu, A. Strybulevych, J. H. Page, S. E. Skipetrov, and van B. A. Tiggelen, Localization of ultrasound in a three-dimensional elastic network, *Nat. Phys.* **4**, 945 (2008).
- [5] J. Billy, V. Josse, Z. Zuo, A. Bernard, B. Hambrecht, P. Lugan, D. Clément, L. Sanchez-Palencia, P. Bouyer, and A. Aspect, Direct observation of Anderson localization of matter waves in a controlled disorder, *Nature (London)* **453**, 891 (2008).
- [6] V. Khemani, R. Nandkishore, and S. L. Sondhi, Nonlocal adiabatic response of a localized system to local manipulations, *Nat. Phys.* **11**, 560 (2015).
- [7] D. L. Deng, J. H. Pixley, X. Li, and S. Das Sarma, Exponential orthogonality catastrophe in single-particle and many-body localized systems, *Phys. Rev. B*, **92**, 220201(R) (2015).
- [8] N. F. Mott and A. E. Davis, *Electronic Processes in Non-Crystalline Materials* (Clarendon, Oxford, 1971).
- [9] Z. Ovadyahu, Optical excitation of electron glasses, *Phys. Rev. B* **83**, 235126 (2011).
- [10] A. Vaknin, Z. Ovadyahu, and M. Pollak, Evidence for Interactions in Nonergodic Electronic Transport, *Phys. Rev. Lett.* **81**, 669 (1998).
- [11] R. Misra, M. McCarthy, and A. F. Hebard, Electric field gating with ionic liquids, *Appl. Phys. Lett.* **90**, 052905 (2007).
- [12] C. C. Yu, Time-Dependent Development of the Coulomb Gap, *Phys. Rev. Lett.* **82**, 4074 (1999); M. Müller and L. B. Ioffe, Glass Transition and the Coulomb Gap in Electron Glasses, *ibid.* **93**, 256403 (2004); V. Malik and D. Kumar, Formation of the Coulomb gap in a Coulomb glass, *Phys. Rev. B* **69**, 153103 (2004); E. Lebanon and Markus Müller, Memory effect in electron glasses: Theoretical analysis via a percolation approach, *ibid.* **72**, 174202 (2005); M. Müller and E. Lebanon, History dependence, memory and metastability in electron glasses, *J. Phys. IV* **131**, 167 (2005); A. Amir, Y. Oreg, and Y. Imry, Mean-field model for electron-glass dynamics, *Phys. Rev. B* **77**, 165207 (2008); Electron glass dynamics, *Annu. Rev. Condens. Matter Phys.* **2**, 235 (2011); Y. Meroz, Y. Oreg, and Y. Imry, Memory effects in the electron glass, *Europhys. Lett.* **105**, 37010 (2014); M. Pollak, M. Ortuño, and A. Frydman, *The Electron Glass* (Cambridge University, England, 2013).
- [13] A. Vaknin, Z. Ovadyahu, and M. Pollak, Non-equilibrium field effect and memory in the electron-glass, *Phys. Rev. B* **65**, 134208 (2002).
- [14] Z. Ovadyahu, Electron-glass in a three-dimensional system, *Phys. Rev. B* **90**, 054204 (2014).
- [15] I. M. Lifshitz and V. Y. Kirpichenkov, Tunnel transparency of disordered systems, *Zh. Eksp. Teor. Fiz.* **77**, 989 (1979) [*Sov. Phys. JETP* **50**, 499 (1979)].
- [16] M. Ya. Azbel, Eigenstates and properties of random systems in one dimension at zero temperature, *Phys. Rev. B* **28**, 4106 (1983).
- [17] J. B. Pendry, Quasi-extended electron states in strongly disordered systems, *J. Phys. C* **20**, 733 (1987).
- [18] Z. Ovadyahu, Slow dynamics of the electron-glasses: The role of disorder, *Phys. Rev. B* **95**, 134203 (2017).
- [19] For the SiO₂ spacer thickness $\delta = 2 \mu\text{m}$ used in these experiments and the thickness of the screening length $\lambda \approx 2 \text{ nm}$, the δV at the sample-interface layer is $\approx 10^{-3} \times (\delta V_g)$.
- [20] O. Faran and Z. Ovadyahu, Magneto-conductance in the variable range hopping regime due to a quantum interference mechanism, *Phys. Rev. B* **38**, 5457 (1988).
- [21] Z. Ovadyahu, Quantum coherent effects in Anderson insulators, *Waves Random Media* **9**, 241 (1999).

- [22] A. Vaknin, A. Frydman, and Z. Ovadyahu, Excess conductance in normal-metal/superconductor junctions, *Phys. Rev. B* **61**, 13037 (2000).
- [23] J. J. Lin and J. P. Bird, Recent experimental studies of electron dephasing in metal and semiconductor mesoscopic structures, *J. Phys.: Condens. Matter* **14**, R501 (2002), and references therein.
- [24] Ya. M. Blanter, Electron-electron scattering rate in disordered mesoscopic systems, *Phys. Rev. B* **54**, 12807 (1996); D. M. Basko, I. L. Aleiner, and B. L. Altshuler, Metal-insulator transition in a weakly interacting many-electron system with localized single-particle states, *Ann. Phys. (NY, U.S.)* **321**, 1126 (2006); I. V. Gornyi, A. D. Mirlin, and D. G. Polyakov, Interacting Electrons in Disordered Wires: Anderson Localization and Low- T Transport, *Phys. Rev. Lett.* **95**, 206603 (2005).
- [25] Z. Ovadyahu, Suppression of Inelastic Electron-Electron Scattering in Anderson Insulators, *Phys. Rev. Lett.* **108**, 156602 (2012).
- [26] E. Yamaguchi, H. Aoki, and H. Kamimura, Intra- and interstate interactions in Anderson localised states, *J. Phys. C* **12**, 4801 (1979).
- [27] B. I. Shklovskii and B. Z. Spivak, Scattering and interference effects in variable range hopping conduction, in *Hopping Transport in Solids*, edited by M. Pollak and B. Shklovskii, Modern Problems in Condensed Matter Sciences Vol. 28 (Elsevier, 1991), Chap. 9; B. Z. Spivak, Anomalous spin magnetoresistance in the region of variable-range hopping conductivity, *Zh. Eksp. Teor. Fiz.* **87**, 1371 (1984) [*Sov. Phys. JETP* **60**, 4 (1984)]; K. V. Kavokin, Spin relaxation of localized electrons in n-type semiconductors, *Semicond. Sci. Technol.* **23**, 114009 (2008).